# Brillouin Scattering Studies of Polymeric Nanostructures*

R. HARTSCHUH,[1] Y. DING,[1] J. H. ROH,[1] A. KISLIUK,[1] A. P. SOKOLOV,[1] C. L. SOLES,[2] R. L. JONES,[2] T. J. HU,[2] W. L. WU,[2] A. P. MAHOROWALA[3]

[1]Department of Polymer Science, University of Akron, Akron, Ohio 44325

[2]Polymers Division, National Institute of Standards and Technology, Gaithersburg, Maryland 20899-8541

[3]IBM T. J. Watson Research Center, Yorktown Heights, New York 10598

*Received 23 September 2003; accepted 29 October 2003*

**ABSTRACT:** For a range of applications, polymers are now being patterned into nanometer-sized features. In these applications, the robust mechanical properties of the nanostructures are critical for performance and stability. Brillouin light scattering is presented as a nondestructive, noncontact tool used to quantify the elastic constants in such nanostructures. We demonstrate this through a series of thin films and parallel ridges and spacings (gratings) with ridge widths ranging from 180 to 80 nm. For the set of films and structures presented here, the room-temperature elastic moduli did not change with decreasing film thickness or grating ridge width, and this implied that one-dimensional and two-dimensional confinement-induced changes of the mechanical properties were not significant down to feature sizes of 80 nm. Additionally, Brillouin spectra of submicrometer gratings revealed new modes not present in the spectra of thin films. The origin of these new modes remains unclear. © 2004 Wiley Periodicals, Inc.† J Polym Sci Part B: Polym Phys 42: 1106–1113, 2004

**Keywords:** Brillouin scattering; polymeric nanostructures; thin polymer films; nanotechnology; mechanical properties; light scattering

## INTRODUCTION

The emerging field of nanotechnology is largely predicated on the ability to construct mechanical, electrical, and optical devices with submicrometer dimensions. Whether these devices consist of polymers, ceramics, or metals, polymers are commonly used in the fabrication or templating process. Processes in which polymers are used at nanometer length scales include deep ultraviolet (UV) lithography, imprint lithography, and molecular self-assembly. Working with materials at submicrometer length scales can be a challenge because many material properties deviate from their bulklike behavior when the materials are confined to small structures or geometries. One good example is the glass-transition temperature ($T_g$) of a polymer, the temperature at which the modulus typically decreases by two or three orders of magnitude. Several studies have indicated appreciable $T_g$ shifts when the film thickness approaches 100 nm or less.[1–4]

In the semiconductor industry, deep UV lithography is routinely used to create nanostructures in polymeric photoresist films, examples of which are shown in Figure 1. The elastic modulus of these polymeric lines is of primary importance because the material from the trenches is dissolved with an aqueous base and rinsed clean

*Contribution from the March 2003 Meeting of the American Physical Society—Division of Polymer Physics, Austin, Texas

*Correspondence to:* C. L. Soles (E-mail: csoles@nist.gov)

Journal of Polymer Science: Part B: Polymer Physics, Vol. 42, 1106–1113 (2004)

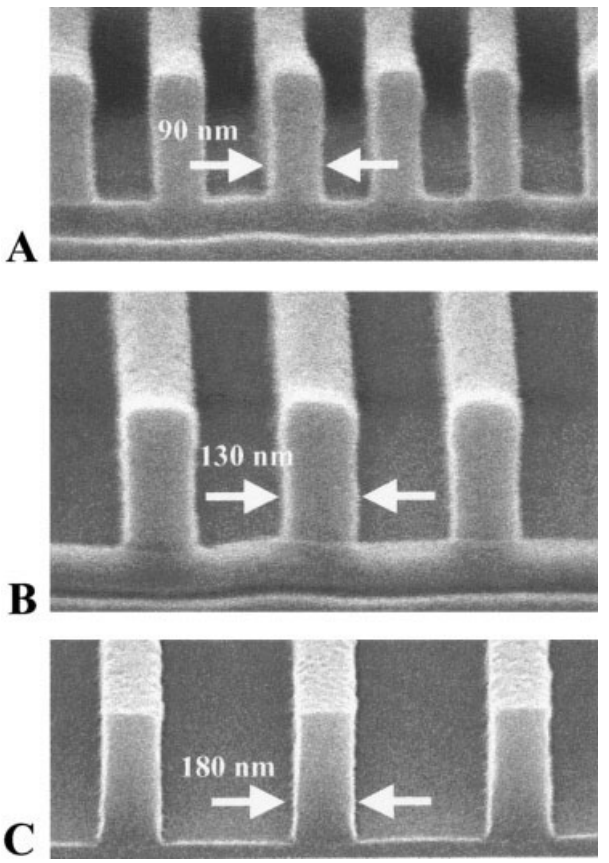


**Figure 1.** SEM images of 193-nm lithography photoresist gratings with line widths of (a) 90 and (b) 130 nm and of a 248-nm lithography photoresist grating with a line width of (c) 180 nm. The thickness of the unpatterned resist film can be inferred from the feature heights.

with deionized water. Drying the water off of the structures eventually leads to a liquid meniscus in the channels between the polymeric walls. The tight radius of curvature of this meniscus generates large Laplace pressures that tend to collapse the structures.[5–7] It has been shown that there is a critical height-to-width aspect ratio for the structures above which pattern collapse becomes an issue.[6,7] In the semiconductor industry, in which the minimum feature widths are now approximately 100 nm, this critical aspect ratio is approximately 3:1.[6,7] However, it is well understood that a higher modulus structure enhances the resistance to collapse.[6,7]

It is critical to create high-aspect-ratio features in lithographic films, especially in the semiconductor industry. The polymeric pattern serves as a template for the desired features, which are etched into the $SiO_2$ substrate by the bombardment of the film with a reactive ion gas. The polymeric pattern temporarily prevents etching of the underlying substrate while the exposed $SiO_2$ is etched away. However, the reactive ion gas also etches the polymer faster than the hard Si substrate. This means that the height of the resist features must be several times greater than the desired etch depth in the substrate. For this reason, one typically maximizes the feature height of the polymer template. This is limited, however, by the increased propensity for pattern collapse. If the modulus is compromised because of confinement, lower aspect ratio features (shallower depths in Si) will be feasible.

Determining the elastic modulus of a relatively soft nanometer-sized feature on a rigid substrate is challenging. Mechanical techniques, such as nanoindentation, typically overestimate properties because of interactions with the rigid substrate.[8–10] There are surface acoustic wave techniques, but thus far these have been used in smooth films, not patterned structures. In this article, we introduce Brillouin scattering for measuring the elastic modulus in lithographically prepared polymer nanostructures supported on a rigid substrate. These measurements somewhat resemble previous studies of the surface acoustic modes in Si surfaces patterned with shallow, submicrometer holographic gratings,[11,12] except that we are measuring deep patterns in a supported film of a distinctly different material. The advantage of Brillouin scattering over mechanical techniques is that it is a noncontact, nondestructive optical technique based on the scattering of laser light by thermal acoustic phonons. By monitoring both the momentum transfer and frequency of the scattered radiation, one can determine the velocity of sound in the structures and, therefore, the elastic modulus.

## EXPERIMENTAL

Brillouin scattering was used to measure the elastic modulus of confined polymers in both smooth films [one-dimensional (1D) confinement] and a series of thin rectangular strips or ridges [two-dimensional (2D) confinement] aligned parallel into gratings. For the smooth films, polystyrene (PS; National Institute of Standards and Technol-

ogy Standard Reference Material 705, $M_w$* = 179 kg/mol and $M_n$ = 171 kg/mol) was dissolved in toluene at various mass fractions and filtered through a 0.45-$\mu$m Teflon filter. The solutions were spin-cast onto Si wafers primed with hexamethyldisilizane, and this created a visibly hydrophobic Si surface. After the spin casting, the films were annealed for 1 h at 135 °C in a vacuum of approximately 5 Pa to remove residual toluene. The film thickness after vacuum annealing, as determined from specular X-ray reflectivity, ranged from 1150.0 to 358.5 nm.

Deep UV lithography was used to fabricate large arrays of parallel photoresist ridges on a Si wafer. The scanning electron microscopy (SEM) images in Figure 1 show three representative gratings, with ridge widths of approximately 90 [Fig. 1(a)], 130 [Fig. 1(b)], and 180 nm [Fig. 1(c)]. Two different forms of deep UV lithography were used to create the structures studied here: 248-nm lithography was used to create the 180-nm ridges separated by 360-nm spacings shown in Figure 1(c), whereas 193-nm lithography was used to fabricate a series of equal lines and spacings with ridge widths varying from 130 to 80 nm. The 248- and 193-nm lithography techniques are based on different commercial photoresists. For all of the structures, there were both patterned (gratings) and unpatterned (smooth film) regions on the wafer so that elastic properties under 2D and 1D confinement could be compared.

Brillouin scattering spectra of the films and gratings were measured in backscattering geometry with a tandem Fabry–Perot interferometer (Sandercock model[13]) and an argon-ion laser (Lexel 3500 with a frequency lock mode) with a wavelength of $\lambda$ = 514.5 nm and 100 mW of power. The free spectral range of the interferometer was set to 25 GHz. The laser spot size was about 30 $\mu$m, that is, an area covering about 100 ridges of the gratings. The polarization of the incident light was horizontal (to the scattering plane), and no analyzer was used for the scattered light. Samples were measured at several different scattering angles ($\theta$) between the film surface normal and the incident light. By changing the incident angle, we adjusted the magnitude of the wavevector parallel to the film surface [$\mathbf{Q} = (4\pi \sin \theta)/\lambda$]. Several of the measurements were performed at a small angle of $\theta = 8°$ ($\mathbf{Q} \approx 3.4\ \mu m^{-1}$) with ridges of the grating oriented perpendicularly to $\mathbf{Q}$. Because of the diffracted light, a strong elastic line appeared in the Brillouin spectra of gratings oriented parallel to $\mathbf{Q}$ at $\theta = 8°$, and no detailed measurements were performed in this geometry. Measurements were also performed at larger angles for both orientations of ridges (parallel and perpendicular to $\mathbf{Q}$) at angles of $\theta = 45°$ ($\mathbf{Q} = 17.3\ \mu m^{-1}$), $\theta = 60°$ ($\mathbf{Q} = 21.2\ \mu m^{-1}$), and $\theta = 67°$ ($\mathbf{Q} = 22.6\ \mu m^{-1}$) for the analysis of the surface Rayleigh modes. The Brillouin peak positions were estimated through the fitting of the spectra with multiple Lorentzians with Origin 6.1 (Microcal) software.

Small-angle X-ray scattering to measure the critical dimensions of the gratings (CD-SAXS) was performed with the 9-ID beam line at the Advance Photon Source at Argonne National Laboratory. With sufficiently high-energy X-rays (13 keV), the measurements were performed in transmission (through the Si substrate) without modification of the samples being required. The beam direction was set normal to the surface plane, and the transmitted scattered intensity was collected on a 2D X-ray detector. Patterns were characterized by the position and relative intensity of the diffraction peaks. Data were reduced to a 1D form by the extraction of the intensity along a line through the diffraction peak maxima after subtraction of the empty beam scattering and correction for dark current noise. Because the diffraction pattern was symmetric around the beam center, positive and negative orders of diffraction were averaged together to increase the signal-to-noise ratio. The data were modeled with an analytical solution of a repeating line grating composed of lines with a rectangular cross section. The shape of the diffraction peaks was modeled with a pseudo-Voigt function, and the decay of the peak intensities with $\mathbf{Q}$ was modeled with a Debye–Waller factor.

## RESULTS AND DISCUSSION

Figure 2 presents Brillouin spectra of bulk PS and several different films of various thicknesses. The spectrum of the bulk sample shows a single longi-

*According to ISO 31-8, the term "molecular weight" has been replaced by "relative molecular mass," symbol $M_r$. Thus, if this nomenclature and notation were to be followed in this publication, one would write $M_{r,w}$ instead of the historically conventional $M_w$ for the mass average molecular weight, with similar changes for $M_n$, $M_z$, and $M_v$, and it would be called the "mass average relative molecular mass." The conventional notation, rather than the ISO notation, has been employed for this publication.

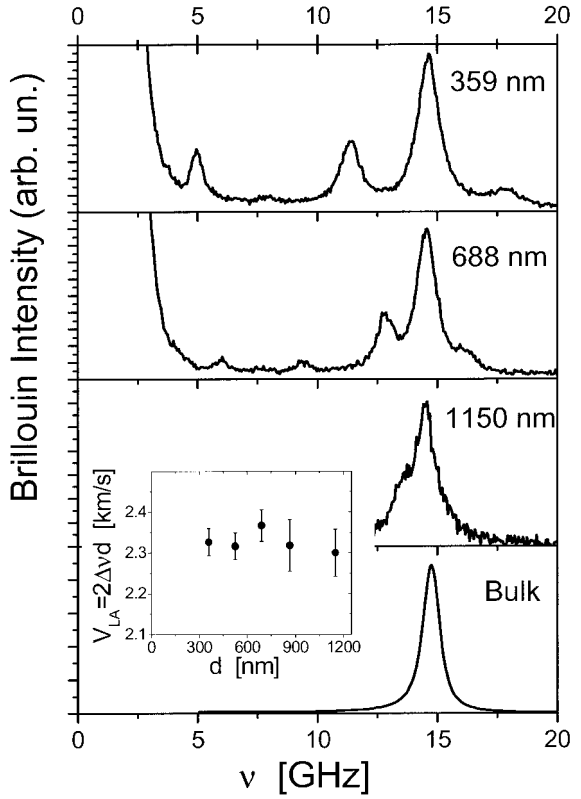


**Figure 2.** Brillouin spectra of bulk and unpatterned PS films as a function of the film thickness measured at $\theta \approx 8°$ ($\mathbf{Q} \approx 3.4\ \mu m^{-1}$). The inset shows the longitudinal sound velocity ($V_{LA}$) estimated from the split energy as a function of $d$.

tudinal acoustic (LA) mode that appears in our backscattering geometry at a certain frequency ($\nu$):

$$\nu \approx 2\frac{nV}{\lambda} \tag{1}$$

where $n$ and $V$ are the refractive index and longitudinal sound velocity of the material, respectively. The frequency at which the LA mode is observed depends on the wavevector $\mathbf{Q}$ of the scattering geometry. There is a continuous distribution in the phonon spectrum, but only those modes with $\mathbf{Q}$ equal to the scattering wavevector are observed (this is analogous to Bragg scattering from crystalline planes). In contrast, many modes can be observed in the spectra of thin films. The reason for the multiple modes is twofold. First, the spectrum of phonons with the wavevector perpendicular to the film surface becomes discrete (quantized) because of limitations in the thickness ($d$):[14]

$$m\lambda_m = m\frac{V}{\nu_m} = 2d \tag{2}$$

where $m$ is an integer number and $\lambda_m$ and $\nu_m$ are the wavelength and frequency of the phonon, respectively. Second, the decrease in the scattering volume broadens the $\mathbf{Q}$-selection rules by $\sin^2(x)/x^2$, where $x$ is equal to $\pi d/\lambda$.[14] Together, these factors explain the presence of many modes of $\nu_m$ in the Brillouin spectrum of the thin films (Fig. 2). These are so-called longitudinal guided modes (LGMs) confined to the thin films.[15,16] If the surface of the film is perpendicular to the incident light, the energy split ($\Delta\nu$) between two neighboring LGM peaks (eq 2) provides an estimate of the sound velocity:

$$\Delta\nu = \nu_m - \nu_{m-1} \approx \frac{V}{2d} \tag{3}$$

In addition, the surface waves or so-called Rayleigh modes appear in the Brillouin spectra because of ripple effects. The frequency of these Rayleigh surface waves depends on the backscattering angle ($\theta$):[17]

$$\nu \approx \frac{V_R Q}{2\pi} = 2\frac{V_R}{\lambda} Sin\theta \tag{4}$$

where $V_R$ is the phase velocity of the Rayleigh surface wave, which is mostly a shear mode (reflecting the shear modulus). In the case of thin films, when $\mathbf{Q}d$ is approximately 1 or less, surface modes with relatively long wavelengths (long in comparison with the thickness) are probed, and $V_R$ is dominated by the elastic constants of the underlying substrate (Si in this case). However, when $\mathbf{Q}d$ is greater than 3, shorter wavelengths are probed, and $V_R$ primarily reflects the shear modulus of the film. The complete theory of Brillouin scattering in thin films is significantly more complicated, and more details are presented elsewhere.[17,18]

An analysis of the $\Delta\nu$ values of the LGM peaks (inset of Fig. 2) shows that the longitudinal sound velocity does not vary with the PS thickness (at least to within 3%) in films down to $d \approx 360$ nm. This result is not surprising because it agrees with studies on free-standing PS films in which variations were not observed even down to $d = 29$ nm.[19] In this geometry, the frequency of the Rayleigh mode ($\nu_R$) is too low (small $\theta$; see eq 4) to be analyzed in Figure 2.

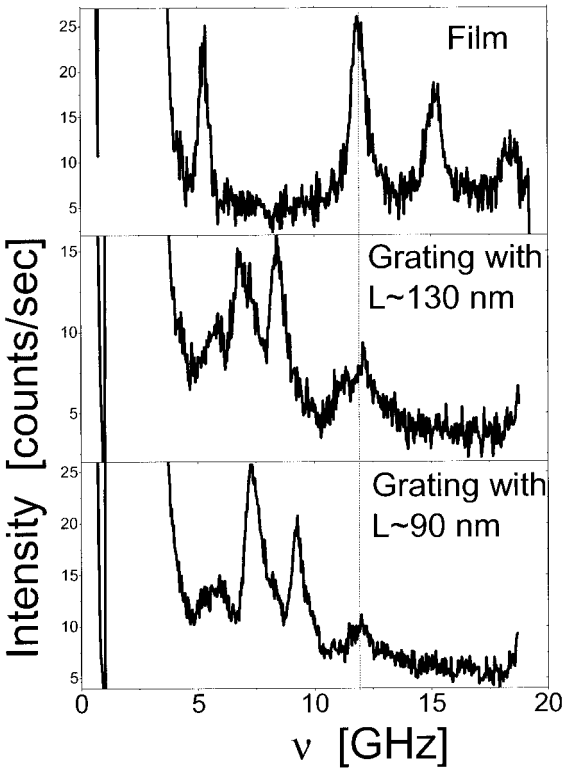


**Figure 3.** Brillouin spectra of 193-nm lithography resist films and gratings with 130- and 90-nm ridge widths measured at $\theta \approx 8°$ ($\mathbf{Q} \approx 3.4\ \mu m^{-1}$). The ridges are aligned perpendicularly to $\mathbf{Q}$. New modes not present in the unpatterned film appear in the spectra of the gratings in the frequency range of 6–10 GHz.

We turn next to the analysis of the Brillouin spectra for the polymeric photoresist films and gratings. A few LGM peaks with $\Delta\nu \approx 3.25$ GHz can be observed in the unpatterned regions of the 193-nm lithography photoresist films (Fig. 3). Measuring a film thickness (i.e., feature height) of $d \approx 300$ nm from the SEM images in Figure 1, we obtain an estimate of the longitudinal sound velocity (with eq 3) of $V \approx 2$ km/s. The frequency of the main LGM peak near 12 GHz remains unchanged (with an accuracy of approximately 3%) for the spectra of the 130- and 90-nm gratings measured under identical conditions in the lower panels of Figure 3. The main LGM peak from the gratings is broadened in comparison with the unpatterned film, probably because of damping of the modes confined in the ridges. Strong scattering of phonons on the side surfaces of the ridges may be one reason for the increased damping.

Tilting the surface normal relative to the incident light, that is, increasing $\mathbf{Q}$, makes the Rayleigh mode in the film and gratings more pronounced (Fig. 4). The Rayleigh mode remains very sharp, even in the gratings, and does not show significant variation either with the dimensions (width) of the ridge or between the patterned and unpatterned regions of the wafer. Figure 5(a) shows $\nu_R$ values measured for a few structures and in the film (unpatterned region). No variation in $\nu_R$ down to a ridge size of approximately 80 nm can be observed. The uncertainties of the frequency are estimated from the averaging of the Stokes and anti-Stokes Rayleigh modes and the uncertainty of $\theta$. The fit gives $V_R = 1.25 \pm 0.03$ km/s for film and submicrometer structures. At $\mathbf{Q}d \approx 6.3$, these $V_R$'s reflect the elasticity of the photoresist and not the underlying substrate. The absence of significant variations in $V_R$ [Figs. 4 and 5(a)], or the frequency of the primary LGM mode (Fig. 3), indicates that the elastic moduli are the same in the smooth films and the patterned features. The formation of narrow ridges with widths down to 80 nm does not affect the moduli of the photoresist.

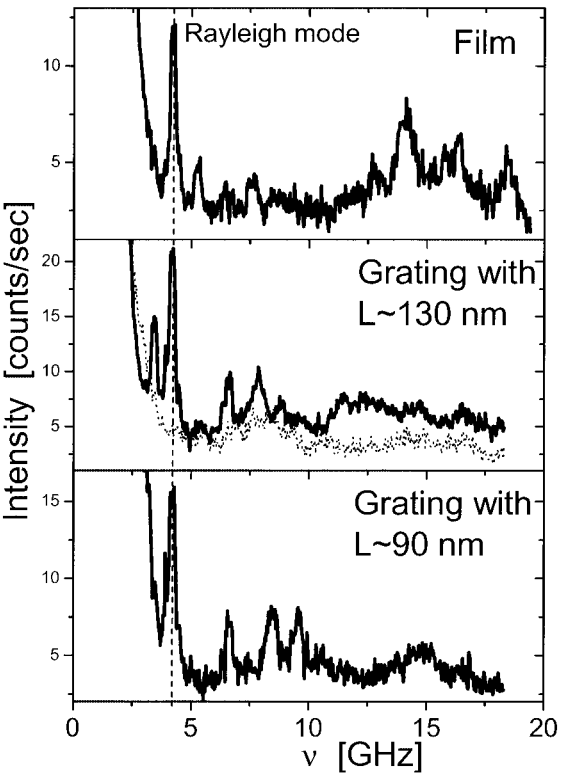


**Figure 4.** Brillouin spectra of a 193-nm lithography resist film and gratings measured at $\theta \approx 60°$ ($\mathbf{Q} \approx 21.2\ \mu m^{-1}$) with the ridges oriented parallel to $\mathbf{Q}$. The dotted line shows the spectrum of the 130-nm grating with the ridges oriented perpendicularly to $\mathbf{Q}$. The Rayleigh mode is indicated by the vertical dashed line.

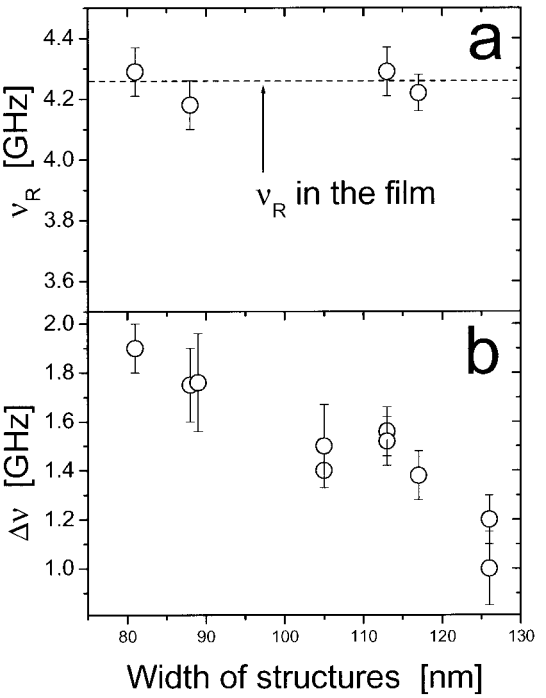


**Figure 5.** Variations of Brillouin frequencies in a series of 193-nm lithography structures as a function of the ridge width: (a) $\nu_R$ values measured at $\mathbf{Q}$ = 22.6 $\mu m^{-1}$ and (b) $\Delta\nu$ values between the additional modes in the gratings at $\mathbf{Q}$ = 3.4 $\mu m^{-1}$ (shown between 6 and 10 GHz in Fig. 3).

Backscattering ($\theta$ = 8°) measurements of the 248-nm lithography photoresist from the unpatterned regions of the film (not shown) give a split of the LGM peaks of $\Delta\nu \approx 2.95$ GHz. With a film thickness of approximately 360 nm, this gives a longitudinal sound velocity of approximately 2.1 km/s. The 193- and 248-nm resists have similar elastic constants in the unpatterned regions of the films. The LGM peaks in 180-nm features are broad and convoluted (Fig. 6), and so we cannot estimate their $\Delta\nu$ values. The reason that the LGMs are less distinct in the 248-nm lithography features (Fig. 6) in comparison with the 193-nm lithography features (Fig. 4) is not immediately evident. However, this breadth may reflect the pattern quality (as discussed later with the help of small-angle X-ray scattering measurements).

The small-angle X-ray scattering measurements of these grating structures reflect the physical quality of the gratings in terms of their periodicity, regularity, and so forth, as described in detail elsewhere.[20] The comparison in Figure 7 indicates that a significantly larger Debye–Waller factor is required to fit the 248-nm resist data with respect to the 193-nm data. The Debye–Waller factor is derived for the limit of small, random deviations of the lines from their lattice positions. In this limit, the factor represents the full width at half-maximum of the distribution of those deviations and is analogous to thermal vibrations of atoms on a crystalline lattice. In this case, however, other defects may produce a similar effect on the scattering and cannot at this time be completely separated. As an example, a deviation in the line shape, such as a trapezoidal cross section, is expected to have a similar result over the measured $\mathbf{Q}$ range. For this reason, we can state (qualitatively only) that a larger Debye–Waller factor is indicative of a decreased quality of patterns, the highest quality pattern being represented by the limit of rectangular cross-section features on a single period lattice. This might suggest that the broad LGMs in Figure 6 reflect less regular features.

The spectra from the 248-nm lithography resist measured at higher angles (higher $\mathbf{Q}$ values) also display sharp Rayleigh modes (Fig. 6). The Rayleigh mode is nearly the same in the film and the grating, in both frequency and width, giving estimates of $V_R$(film) = 1.21 ± 0.02 km/s and $V_R$(180 nm) = 1.24 ± 0.02 km/s. As with the 90- and 130-nm gratings, the unchanging Rayleigh mode suggests that there is no significant difference in the elastic constants between the film and the 180-nm grating.

At high $\mathbf{Q}$ values, rotating the gratings 90° so that the ridges are perpendicular to $\mathbf{Q}$ causes all

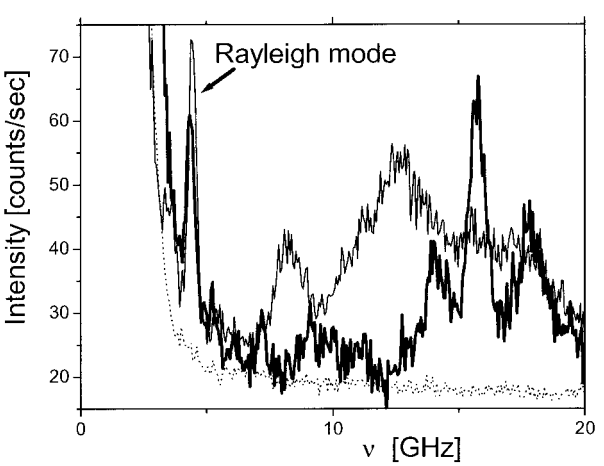


**Figure 6.** Brillouin spectra of a 248-nm lithography resist film (thick, solid line), a 180-nm grating with ridges parallel to $\mathbf{Q}$ (thin, solid line), and a 180-nm grating with ridges perpendicular to $\mathbf{Q}$ (dotted line). The spectra are measured at $\theta \approx 67°$ ($\mathbf{Q} \approx 22.6$ $\mu m^{-1}$), and the Rayleigh mode is indicated.

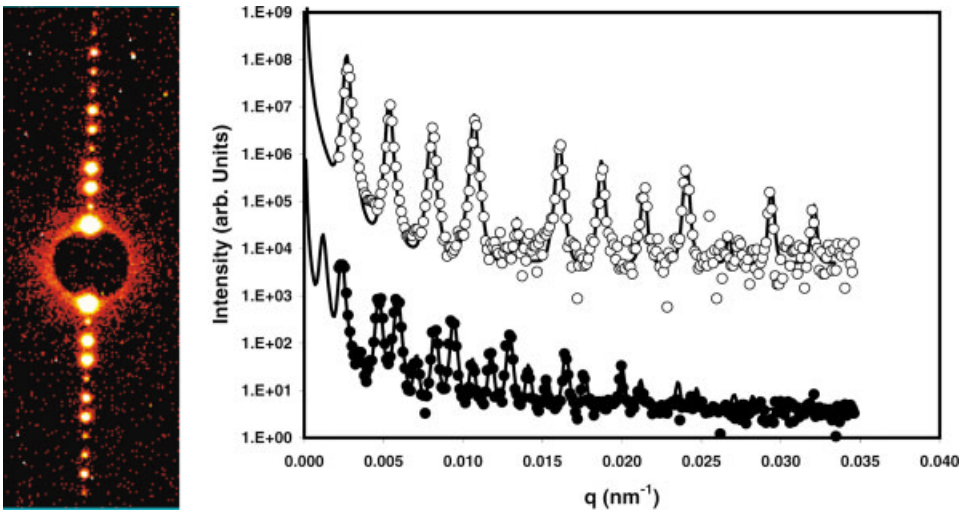


**Figure 7.** Detector image of typical CD-SAXS pattern showing diffraction peaks symmetrically centered at the beam center (left). Also shown are CD-SAXS results comparing the decay rates of the diffraction peak intensity in 248-nm resist structures (filled symbols) and 193-nm resist structures (open symbols). The intensities have been shifted vertically for clarity.

Brillouin peaks to disappear (or at least become strongly suppressed). This is shown in Figures 4 and 6 by the dotted lines. The spectra in both figures are presented as counts/s per channel, and this means that the absolute inelastic scattering intensity decreases sharply for the orientation of ridges perpendicular to **Q**. These spectra are measured with a significant **Q** component, and this means that they probe modes propagating along the direction parallel to **Q**. The disappearance of the peaks in these spectra may be explained by the absence (or strong suppression) of phonons propagating perpendicularly to the grating ridges. These are not surfaces waves propagating over a textured surface. The height of the ridges is larger than their width, and they are separated by a free space of equal or greater width. This is in contrast to reports for shallow gratings (when the depth of the grating is much smaller than its period) produced in Si in which Brillouin spectra due to zone folding have been observed.[11]

An interesting observation is the appearance of additional modes in the spectra of the 90- and 130-nm gratings in the frequency range between 6 and 11 GHz, in which intense modes cannot be seen in the unpatterned regions of the film (Fig. 3). The $\Delta\nu$ value between these additional modes increases with decreasing ridge width [Fig. 5(b)], and this indicates some type of lateral confinement within the ridge. There is also an additional mode resolved below the Rayleigh mode in the 130-nm gratings (Fig. 4). The Brillouin spectra of 180-nm structures (Fig. 6) also show indications of these additional modes. However, they are broad and strongly overlap, and so we cannot estimate their $\Delta\nu$ values. These new modes (both the new modes that split with the ridge width and the additional mode below the Rayleigh mode) were not anticipated or predicted by any existing theory; further experimental and theoretical developments are needed to fully comprehend their origin. Nevertheless, the observed broadening of the LGM modes, the suppression of the spectra measured at high **Q** values with the orientation of ridges perpendicular to **Q**, and the appearance of new modes seem to be general features of the Brillouin spectra of submicrometer polymeric gratings.

## CONCLUSIONS

We have presented Brillouin scattering spectra for a series of polymers confined to both thin films (1D confinement) and lithographically prepared gratings (2D confinement). The Brillouin measurements indicate no change in the elastic moduli of 2D confined polymer photoresists down to sizes as low as 80 nm. New phonon modes that are not seen in the thin-film geometry appear in the spectra of gratings. Their $\Delta\nu$ value increases as the width of the ridges decreases. An under-

standing of the nature of these modes requires deep theoretical analysis and might provide additional information on the mechanical properties of submicrometer structures.

The authors from the University of Akron are grateful for the financial support of the National Institute of Standards and Technology and Air Force Research Laboratory (AFRL). R. Hartschuh thanks Goodyear Tire & Rubber Co. for its financial support of his summer internship at the University of Akron.

## REFERENCES AND NOTES

1. Keddie, J. L.; Jones, R. A. L.; Cory, R. A. Europhys Lett 1994, 27, 59.
2. Forrest, J. A.; Dalnoki-Veress, K.; Dutcher, J. R. Phys Rev E 1997, 56, 5705.
3. Fryer, D. S.; Peters, R. D.; Kim, E. J.; Tomaszewiski, J. E.; de Pablo, J. J.; Nealey, P. F.; White, C. C.; Wu, W.-L. Macromolecules 2001, 34, 5627.
4. Forrest, J. A.; Dalnoki-Veress, K.; Stevens, J. R.; Dutcher, J. R. Phys Rev Lett 1996, 77, 2002.
5. Tanaka, T.; Morigami, M.; Atoda, N. Jpn J Appl Phys 1993, 32, 6059.
6. Namatsu, H.; Kurihara, K.; Nagase, M.; Iwadate, K.; Murase, K. Appl Phys Lett 1995, 66, 2655.
7. Cao, H. B.; Nealey, P. F.; Domke, W.-D. J Vac Sci Technol B 2000, 18, 3303.
8. Murray, C.; Flannery, C. M.; Streiter, I.; Schulz, S. E.; Baklanov, M. R. Microelectron Eng 2002, 60, 133.
9. Van Landingham, M. R.; Villarrubia, J. S.; Guthrie, W. F.; Meyers, G. F. Macromol Symp 2001, 167, 15.
10. Flannery, C. M.; Wittkowski, T.; Jung, K.; Hillebrands, B.; Baklanov, M. R. Appl Phys Lett 2002, 80, 4594.
11. Dutcher, J. R.; Lee, S.; Hillebrands, B.; McLaughlin, G. J.; Nickel, B. G.; Stegeman, G. I. Phys Rev Lett 1992, 68, 2464.
12. Giovannini, L.; Nizzoli, F.; Marvin, A. M. Phys Rev Lett 1992, 69, 1572.
13. Certain commercial equipment and materials are identified in this article to specify adequately the experimental procedure. In no case does such identification imply recommendation by the National Institute of Standards and Technology nor does it imply that the material or equipment identified is necessarily the best available for this purpose.
14. Sandercock, J. R. Phys Rev Lett 1972, 29, 1735.
15. Hillebrands, B.; Lee, S.; Stegeman, G. I.; Cheng, H.; Potts, J. E.; Nizzoli, F. Phys Rev Lett 1988, 60, 832.
16. Nizzoli, F.; Hillebrands, B.; Lee, S.; Stegeman, G. I.; Duda, G.; Wegner, G.; Knoll, W. Phys Rev B. 1989, 40, 3323.
17. Nizzoli, F.; Sandercock, J. R. In Dynamical Properties of Solids; Horton, G. K.; Maradudin, A. A., Eds.; Elsevier: Amsterdam, 1990; Vol. 6, p 281.
18. Hotz, R.; Kruger, J. K.; Possart, W.; Tadros-Morgane, R. J Phys: Condens Matter 2001, 13, 7953.
19. Forrest, J. A.; Dalnok-Veress, K.; Dutcher, J. R. Phys Rev E 1998, 58, 6109.
20. Jones, R. L.; Hu, T. J.; Lin, E. K.; Wu, W.-L.; Kolb, R.; Casa, D. M.; Bolton, P. J.; Barclay, G. G. Appl Phys Lett, 2003, 83, 4059.